

Intergalactic Filaments as Isothermal Gas Cylinders

A. Gayler Harford¹ and Andrew J. S. Hamilton^{1,2}

¹*JILA, University of Colorado, Boulder, CO 80309, USA*

²*Dept. Astrophysical & Planetary Sciences, University of Colorado, Box 440, Boulder CO 80309, USA*

1 June 2019

ABSTRACT

Using a cosmological simulation at redshift 5, we find that the baryon-rich cores of intergalactic filaments radiating from galaxies commonly form isothermal gas cylinders. The central gas density is typically about 500 times the cosmic mean total density, and the temperature is typically 1-2 times 10^4 K, just above the Lyman alpha cooling floor. These findings argue that the hydrodynamic properties of the gas are more important than the dark matter in determining the structure. Filaments form a major pipeline for the transport of gas into the centers of galaxies. Since the temperature and ionization state of the gas completely determine the mass per unit length of an isothermal gas cylinder, our findings suggest a constraint upon gas transport into galaxies by this mechanism.

Key words: cosmology: theory – intergalactic – filaments – sheets – baryons

1 INTRODUCTION

The standard model of cosmology emphasizes the role of the gravitational field of the dark matter in structure formation. In this picture, the dark matter determines the overall geometry and rate of growth of structure.

While analyzing a cosmological simulation at redshift 5, we found that on scales of a few proper kiloparsecs intergalactic dark matter and baryons form qualitatively different structures (Harford et al. 2008). In contrast to the dark matter, which tends to occur in many small, quasi-spherical clumps, the baryons occur in a framework of thin, smooth rods that form backbones connecting the large, dark matter dominated galaxies.

These gaseous filaments likely correspond to the filaments described by others that mediate the “cold mode” mechanism of gas transport into galaxies (Birnboim & Dekel 2003; Katz et al. 2003; Kereš et al. 2005; Dekel & Birnboim 2006; Kawata & Rauch 2007; Ocvirk et al. 2008; Kereš et al. 2009; Dekel et al. 2009; Brooks et al. 2009). The structure of our filaments might then have ramifications for understanding how galaxies gain the gas necessary for the varied star formation histories that are observed.

We reasoned that these contrasting distributions of gas and dark matter result from hydrodynamic effects: pressure forces retard the gas as it moves toward the axis of a filament, in contrast to the dark matter which can pass freely through subject only to gravitational forces. The gas would be expected to accumulate along the axis of the filament until the pressure forces are sufficient to counteract the

gravitational field. In this paper we explore the hypothesis that the gas in the baryonic core forms an isothermal cylinder whose structure is determined primarily by the gravitational and hydrodynamic properties of the gas.

Many different versions of an isothermal cylinder are possible with different degrees of concentration of the gas, but they all share the interesting property that the total mass per unit length of the gas depends only on the temperature and ionization state of the gas (Stodólkiewicz 1963; Ostriker 1964). We suggest that our findings place constraints upon models for the movement of gas along filaments.

The importance of hydrodynamic forces for the filament structure supports a hydrodynamic mechanism of origin from isothermal sheets as first proposed by Schmid-Burgk (1967).

2 RATIONALE

In Paper I (Harford et al. 2008) we studied the distributions of dark matter and baryons in a detailed cosmological simulation run to a redshift of 5.1. At this redshift we found that the distributions of dark matter and baryons begin to diverge in an interesting way at a scale less than 40 kpc comoving. Dividing the simulation box into cubical grid cells of this dimension, we found that among cells with a total overdensity of $10^{1.75}$ or greater, about 5% have a baryonic fraction exceeding twice the cosmic mean. These enriched cells, in contrast to their unenriched peers, form a network of long, thin filaments that connect the largest galaxies. We

studied the filaments extending from the ten largest galaxies in detail and found that, in addition to being baryon-rich, they radiate in approximately straight lines from the centers of the galaxies.

Since the movement of gas along filaments has been shown by others to be an important mechanism for the addition of gas to galaxies, we decided to study the structure of these filaments in more detail.

Our working hypothesis is that the filaments form isothermal cylinders that extend in straight lines from the centers of galaxies. Filaments in a cosmological simulation are of course messier than this idealization. They may be bent, truncated, or disturbed in various ways by galaxies, small dark matter haloes, or other filaments. Thus at best it can be shown only that relatively undisturbed filaments emanating from galaxies are commonly reasonably well approximated as isothermal cylinders. Despite this limitation, such a finding would be interesting because it would suggest that the dynamics of filaments at scales of a few kpc at redshift 5 is dominated by gaseous processes rather than by the gravity of dark matter.

In anticipation of considerable variability, we expanded our study to include the filaments around the 200 largest galaxies in the simulation. These galaxies range in total mass from $10^{9.70} M_{\odot}$ to $10^{11.07} M_{\odot}$.

We used the same simulation at the same redshift as in Paper I. A feature that distinguishes this simulation from many others in the literature is that the ionizing radiation is generated self-consistently from the simulated star formation rather than added as a uniform background. Detailed chemistry and radiative transfer computations are included. Resultant luminosity functions are reasonable (Harford & Gnedin 2003, 2007). Although the history of reionization remains controversial, the process within the simulation is at least consistent with the spectra of high-redshift quasars (Gnedin & Fan 2006). The importance of the latter is underscored by the finding that the Jeans length changes by more than an order of magnitude over the course of reionization (see Gnedin et al. 2003 and references therein).

In what follows, all distances are proper unless specified otherwise. All histograms are shown with the plotted point at the center of the bin.

3 OVERVIEW OF ANALYSIS

To study a large number of galaxies, we devised an efficient, objective way to identify filaments. In Paper I we found that the baryon-rich filaments extend from the centers of the galaxies in a predominantly radial direction, consistent with their being conduits for gas accretion onto galaxies. From this perspective, we take as our defining feature of a filament a long, straight rod of gas protruding from the center of a galaxy.

To implement this definition we used the HealPix (Górski et al. 2005) partition of the volume of a sphere centered on each galaxy. This method divides the region completely into volume elements of equal solid angle issuing from the center. We reasoned that the volume elements containing the most gas probably represent directions of filaments.

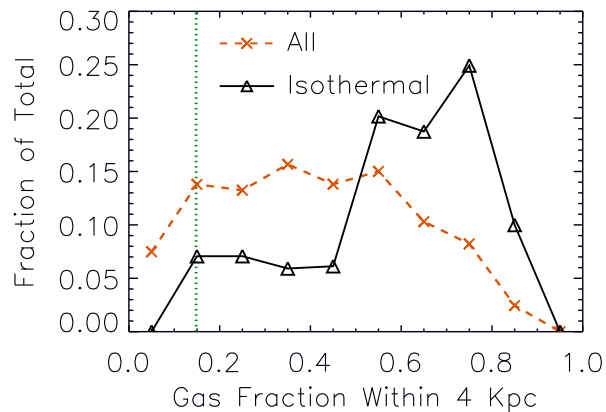


Figure 1.

Gas fractions of segments. Dashed, orange line with X's represents all candidates segments. Solid, black line with triangles represents the isothermal cylinders identified. The vertical, green, dotted line marks the mean cosmic baryon fraction. The gas fraction is computed for all matter within 4 kpc of the axis of the segment. Stellar particles are combined with dark matter for this computation since they are treated as collisionless in the simulation.

To allow for the possibility that the filament structure might vary along its length, we divided each filament into segments for individual analysis. Each segment is bracketed by two concentric spheres centered on the galaxy. We refer to the region between the two spheres as the parent shell of the segment. We will show in section 4.6 that the structure of the segment depends upon the density of the parent shell. The four possible segments of a filament that we consider lie in a radial range between about 22 and 50 kpc from the center of the galaxy. This range, which is similar to that used in Paper I, was chosen to be far enough from the galaxy to be usually outside the virial radius and to be not so far away as to run into another galaxy. The implementation of this technique is described in section 4.2.

The technique identifies segments of filaments belonging to a small number of major strings of galaxies, resembling the filaments formed by the baryon-rich grid cells in Paper I. This collection of segments will form the pool of candidates that we will examine for isothermal cylinders.

Figure 1 shows that the cores of the majority of the segments are enriched in gas above the cosmic mean, consistent with the findings of Paper I. The subset of segments that we find to be isothermal is even more gas rich. In the present paper we use the gas fraction rather than the baryonic fraction used in Paper I. This convention was chosen because the stellar particles in the simulation, like the dark matter ones, are treated as collisionless, in contrast to the hydrodynamic treatment of the gas. The contribution of stars to the baryonic fraction is generally small.

The segments have average temperatures of about 12000 to 14000 K, just above the Lyman alpha cooling floor (Figure 2) and neutral hydrogen fractions of about 0.01 to 0.02 (Figure 3).

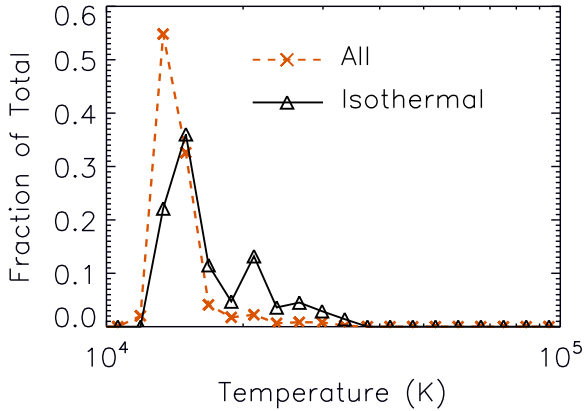


Figure 2. Histogram of average gas temperatures of segments. Dashed, orange line with X's represents all candidate segments. Solid line with triangles represents the isothermal segments identified in this study. The temperature was averaged by mass for the gas within 4 kpc of the axis of the cylinder.

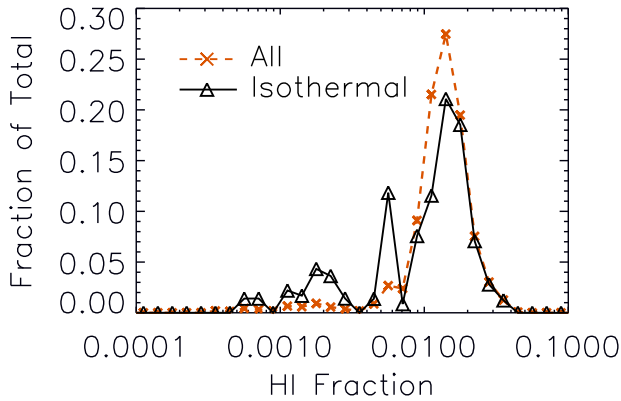


Figure 3. HI fractions of hydrogen in segments. The HI fraction was averaged by mass for the region within 4 kpc of the axis of the segment. Dashed, orange line with X's represents all candidate segments. Solid, black line with triangles the isothermal ones.

The structure of each segment was determined from the cylindrical, radial profile of the gravitational potential produced by the distribution of its gas. Section 4.3 describes the basic properties of an isothermal cylindrical potential. Details of the computation and the fitting of the potential profiles to an isothermal one are given in sections 4.4 and 4.5.

From an isothermal potential profile, an effective sound speed can be computed. This is the sound speed that the gas would need to have to balance its gravitational field. The effective sound speed is then compared to the actual average sound speed of the gas, which depends upon the temperature and ionization state of the gas. Those candidates whose potential profile fits an isothermal one for some effective temperature will be referred to as isothermal-like. Of these,

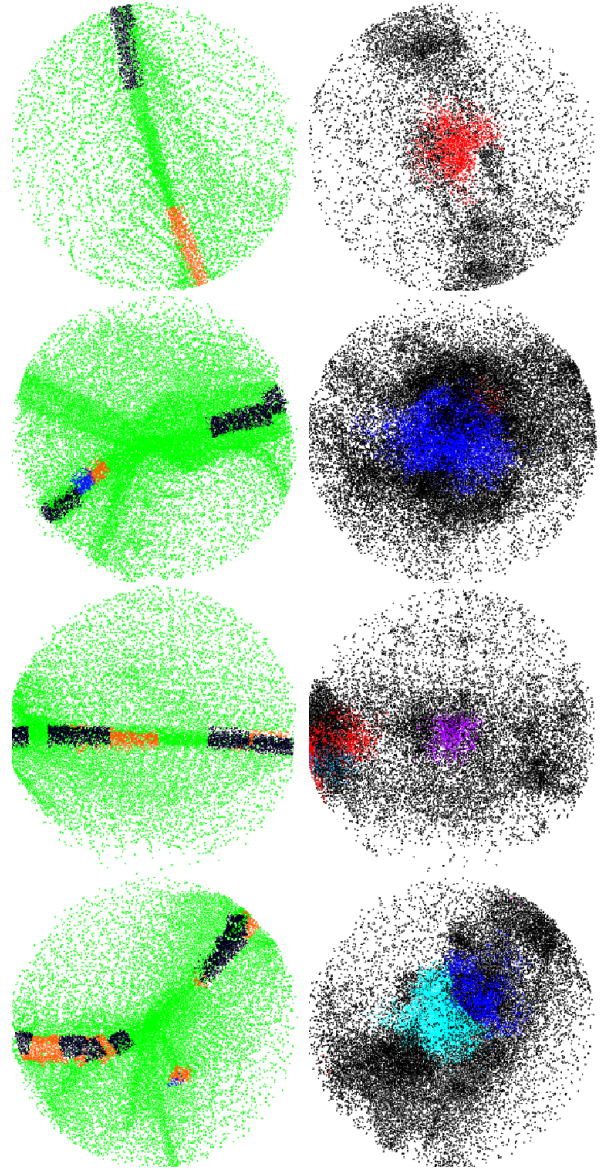


Figure 4. Typical images of gas and dark matter around four galaxies. Each row shows two images of the same view of a sphere of radius about 51 kpc centered on a single galaxy. The left image of each pair shows just the gas particles with those within 4 kpc of the axis of a segment colored as follows: black isothermal, blue isothermal-like, orange other candidates. All other gas particles are colored green. Overlaps among segments have been eliminated as explained in section 4.6. The right image of each pair shows just the dark matter particles. Here the different colors other than black indicate different galaxies, among the 200 examined, to which the dark matter particle is bound.

Row 1 contains five isothermal segments, which emanate from two galaxies. Row 2 is centered on the largest galaxy. It contains seven isothermal segments, which emanate from three galaxies. Row 3 contains eight isothermal segments, which emanate from three galaxies. Row 4 is centered on the fifth largest galaxy. It has eight isothermal segments, which emanate from six galaxies.

those whose effective temperature agrees with the actual one within a factor of two will be designated as isothermal.

We find empirically that two factors are important in determining whether an isothermal cylinder will be present (section 4.6). The most important one is the total cosmic overdensity of the parent shell around the galaxy in which the segment resides. A value of at least ten seems to be needed, perhaps to ensure that enough gas is present to form an isothermal cylinder at the prevailing temperature. The second factor is the gas fraction of the segment. A gas fraction of at least 0.5 appears to be helpful, perhaps to minimize the perturbing effects of the gravitational field of the dark matter.

Among segments with high (≥ 0.5) gas fractions residing in regions of high (≥ 10) total overdensity, 52% meet our requirements for an isothermal cylinder. Furthermore, among the densest parent shells, those with an overdensity greater than twenty, about 40% host at least one isothermal segment. There are many reasons why an isothermal cylinder that actually exists might fail to be identified in our study. We conclude that isothermal cylinders are at least common under conditions favorable to their formation.

Figure 4 shows images of a sphere of radius 51 kpc centered on each of four galaxies. The left image shows just the gas particles and the right image just the dark matter. These images are typical of those of the 37 galaxies, ranging in total mass from $10^{9.71} M_{\odot}$ to $10^{11.07} M_{\odot}$, from which isothermal segments emanate. The marked contrast in the distribution of gas and dark matter confirms our findings in Paper I.

From the isothermal potential profile we can determine the central density, a useful value that is difficult to compute directly from the gas particles of the simulation. The isothermal segments have central densities equal to about 500 times the mean overall cosmic density, above the value of 200 normally considered indicative of virialization. This result suggests that dark matter is not needed to maintain the structure in the presence of the Hubble expansion. This finding, coupled with the high gas fractions, argues that the structure of these segments is primarily determined by the hydrodynamic properties of the gas rather than by the dark matter.

Since the total mass per unit length of an isothermal cylinder depends only upon the temperature and ionization state of the gas, an upper limit can be placed upon the flux of gas along a filament having this structure.

4 RESULTS

4.1 Review of Simulation

The simulation from which the filaments are drawn is the same as that in Paper I, and has been previously described there. It utilizes a ‘‘Softened Lagrangian Hydrodynamics’’ (SLH-P³M) code (Gnedin 1995; Gnedin & Bertschinger 1996) with a flat Λ CDM cosmology. The cosmological parameters are $\Omega_m = 0.27$, $\Omega_b = 0.04$, $\sigma_8 = 0.91$, and $h = 0.71$. The simulation is developed self-consistently, following the gas dynamics on a quasi-Lagrangian mesh, which deforms adaptively to provide higher resolution in higher density regions. As in Paper I we concentrate on

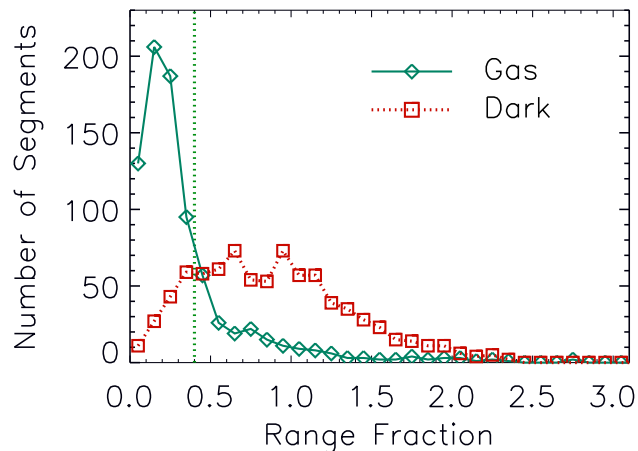


Figure 5. Histogram showing the distribution of gas and dark matter along segments. Solid, blue line with diamonds represents the gas. Dotted, red line with squares represents the dark matter. After dividing the segment longitudinally into three equal parts, a ‘‘range fraction’’ is obtained by dividing the maximum difference in mass between any two parts by the average mass of the three parts. We consider the distribution uniform if the range fraction does not exceed 0.4.

a snapshot of the simulation at a redshift of 5.135. The softening length was 0.08 proper kpc at this redshift. The dark matter particle mass was $2.73 \times 10^6 M_{\odot}$, and the fiducial mass of a gas particle was $4.75 \times 10^5 M_{\odot}$.

4.2 Finding Filaments

To implement our filament definition described in section 3 we used the HealPix¹ partition of the volume of a sphere (Górski et al. 2005) centered on each of 200 galaxies. A subdivision into 768 pixels proved ideal.

Each angular pixel is divided into four radial subpixels corresponding to four spherical shells bracketed by five spheres at 3, 4, 5, 6, and 7 radial units (7.24 kpc) from the center of the galaxy. The minimum distance from the galaxy center is thus 22 kpc, outside the virial radius of all but a few of the larger galaxies. The virial radii range from 28 kpc for the largest galaxy down to 6 kpc².

For our study we selected as possible segments of filaments those subpixels having at least 30 times the average amount of gas per subpixel in the shell. Neighboring subpixels are consolidated into a single peak segment.

We then require that the gas be uniformly distributed along the axis of the segment in order to eliminate galaxies, grossly misaligned filaments, and other miscellaneous oddities. For this test, the segment is divided longitudinally into three parts, and the total gas mass within four kpc of the axis is computed for each. A range fraction is obtained by

¹ We gratefully acknowledge the use of the HealPix software package obtained from <http://healpix.jpl.nasa.gov>.

² The virial radius was taken to be the radius enclosing an average total density of 200 times the cosmic mean.

dividing the maximum difference between any two parts by the average of the three parts. We consider the distribution uniform if the range fraction does not exceed 0.4.

The 618 segments that meet both tests constitute the candidate segments to be examined for isothermal structure. They radiate from 178 of the 200 galaxies analyzed.

The method, though crude, quickly identifies filamentous structures. Visual inspection shows the segments lined up into filaments of up to four segments. On a larger scale the filaments merge to connect many galaxies in a filamentary network.

A corresponding range fraction was computed for the dark matter in these candidate segments. Figure 5 shows that the gas and dark matter are distributed very differently by this criterion.

4.3 Isothermal Cylinders

The infinite, self-gravitating isothermal gas cylinder in hydrodynamical equilibrium has been described mathematically by Stodólkiewicz (1963) and Ostriker (1964). The density profile is given by

$$\rho = \rho_0 \frac{1}{(1 + \frac{1}{8}\xi^2)^2} \quad (1)$$

where ρ_0 is the central density along the axis of the cylinder and ξ is a transverse radial length variable whose unit value, or scale radius, is

$$r_s = \frac{c_s}{\sqrt{4\pi G\rho_0}}. \quad (2)$$

In this expression c_s is the isothermal speed of sound and G is the gravitational constant. The speed of sound depends only upon the temperature T and the mean molecular weight μ

$$c_s = \sqrt{\frac{kT}{\mu m_H}} \quad (3)$$

where k is the Boltzmann constant and m_H is the mass of the hydrogen atom.

Because of the limited number of simulation particles, it is convenient to work with the gravitational potential produced by the distribution of the gas rather than with the density profile itself. Dividing the potential by c_s^2 gives a dimensionless variable ψ which takes the simple form

$$\psi(\xi) = 2 \ln(1 + \frac{1}{8}\xi^2) \quad (4)$$

for the isothermal cylinder.

4.4 Computing the Gas Potential

The gravitational potential generated by the gas of a segment is computed on a 200 x 200 plane grid with a spacing of 0.17 kpc, perpendicular to the segment at its center. The potential is a sum over the contributions of all gas particles within 7 kpc of the cylindrical axis. Using a preliminary computation, this axis is adjusted to the common center of the largest contours, which are nearly concentric circles.

The 7 kpc maximal radius for the gas was chosen from experience, coupled with our findings in Paper I. A

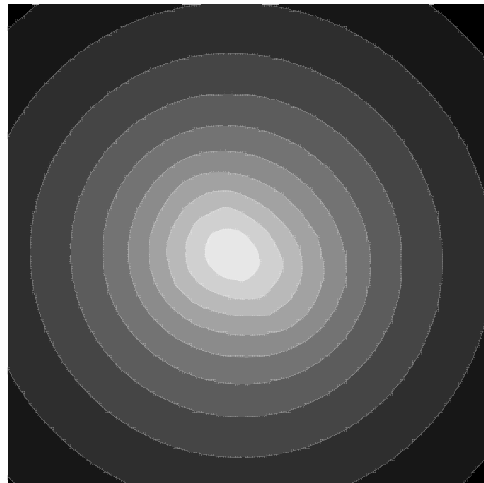


Figure 6. Gas potential contours for a segment of a filament of the largest galaxy. The dimension of image is 34 kpc. The potential is computed from gas within 7 kpc of central axis. Fifty equally spaced contours are computed. For clarity only a few of them are shown here.

softening length of 0.1 kpc is added in quadrature to each contribution. In order to compare the potential of the finite segment to the simple form for an infinite cylinder, the gas particle distribution is replicated ten times in each direction along the axis, and the potential contributions of these additional particles added in.

Fifty equally spaced contours on the full grid are computed, using the IDL Software (Research Systems). Example potential contours are shown in Figure 6.

4.5 Fitting to an Isothermal Potential

The result is a set of contours for a nearly cylindrically symmetric potential well. The average radius of each contour about its own center is used to construct a radial potential profile. As will be shown, the contour centers very nearly coincide.

The zero point for the potential of an isothermal cylinder is defined to be the potential on the cylinder axis (Ostriker 1964). We take as our estimate of this value the value at the most extreme grid point within the innermost contour.

An isothermal potential profile is completely characterized by two parameters, the scale radius and the sound speed. We determined the scale radius for which the profile is the best fit up to a constant of proportionality. The constant for the best fit is then the reciprocal of the square of an “effective” sound speed.

The test region for each trial is a cylindrical shell between one and 4.25 scale radii. This region contains the characteristic inflection point of the potential curve at the square root of eight times the scale radius, a radius enclosing half the total mass of an isothermal cylinder. The central region where small irregularities have a large effect on the profile is thus omitted from the fitting procedure.

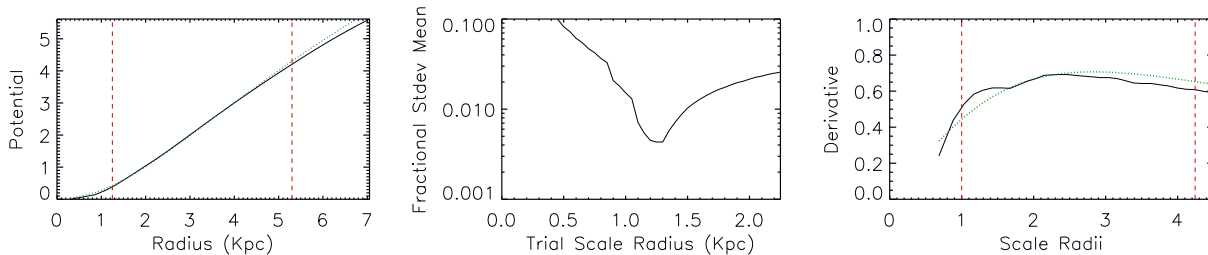


Figure 7. Fitting data for a segment derived from a filament emanating from the largest galaxy in the simulation. In the left and right panels, the dotted, green lines are the theoretical prediction. The vertical, dashed, red lines enclose the fitting region for the optimal fit that is shown.

Left: Best fit of gas potential ψ to theory. Solid, black line is the potential of a segment divided by the square of the best-fit sound speed plotted as a function of radius. See section 4.3 for a definition of ψ .

Center: Delimitation of best fit. Shows the ratio of the standard deviation of the mean of the proportionality constant to the constant itself as a function of the trial scale radius for the segment whose profile is shown on the left.

Right: Fit of the derivative of the gas potential ψ on the left to theory. Solid, black line is the derivative of the gas potential shown in left panel. The abscissa shows the radius as a multiple of the scale radius for this fit.

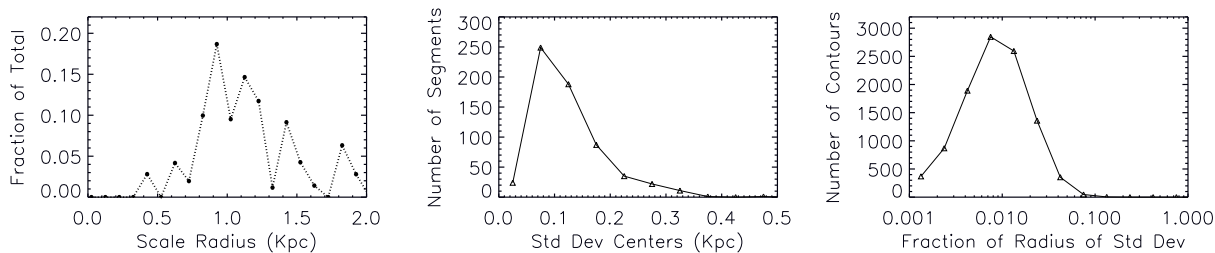


Figure 8. Left: Histogram of scale radii for the isothermal-like segments, that is, those segments having an isothermal profile for some effective temperature.

Center: Test of whether contour centers coincide. Shown is a histogram of the standard deviation of contour centers from mean of the contour centers for each of the candidate segments. Included are all contours from the fitted region corresponding to the best fit. Segments are 7.24 kpc in length and are analyzed individually.

Right: Test of the straightness and cylindrical symmetry of the individual segments. Shown is a histogram of the standard deviation of the mean of the radius of the individual points that make up each contour. The standard deviation is expressed as a fraction of the mean radius of the contour. Included are all candidate segment contours from the fitted region corresponding to the best fit.

For each of a range of scale radii the standard deviation of the mean of the proportionality constant throughout the fitting region is determined. The scale radius for which the ratio of this standard deviation to the constant of proportionality itself is a minimum is taken as the best fitting scale radius. We require the minimum ratio to be less than 0.01 because we find empirically that these fits narrowly prescribe the optimal scale radius. Figure 7, center panel, shows an example of the determination of the optimal scale radius. Fits this good usually show the inflection point well.

Segments that fit this well are then further tested by computing the fractional standard deviation of the fit to the derivative. Here, a cutoff of 0.1 was used. This test eliminates some pathological cases, often involving very small scale radii and thus very small fitting regions. Examples of well-fitting profiles of the potential and its derivative are shown in Figure 7, left and right panels respectively.

As a further test of the fit, the total mass within four scale radii was compared to prediction. The computed mass is invariably smaller than predicted presumably because the centering varies slightly along the axis of the cylinder. Only when all centers coincide would the mass be expected to be

100% that of prediction. We require that the actual mass be at least 70% of prediction. The segments failing this test generally have very small scale radii and thus a small spatial region for the fitting.

Those segments meeting all of these tests are considered to be isothermal-like, that is, they have an isothermal profile for some effective temperature. The number of equally spaced contours in the fitting region for the best fit ranges from about 20 to 35. Figure 8, left panel, shows a histogram of their scale radii. Most are between 0.8 and 1.5 kpc. The low end may be underrepresented because of the small volume of the resultant fitting region. The high end may be underrepresented because the fitting region is slightly truncated in those few cases where it would otherwise extend beyond 7 kpc.

For cylindrical symmetry, the centers of the closed contours should coincide. For the fitted region of each segment the standard deviation of the contour centers about the mean of these centers was computed. Figure 8, center panel, shows a histogram of these standard deviations for all of the segments fitting the isothermal curve and its derivative for some effective temperature. Also for straight cylinders the contours should be nearly circular. Figure 8,

right panel, shows a histogram of the fractional standard deviations of the mean radius for these contours.

4.6 Evaluating the Candidates

The fit allows us to compute for each segment an effective sound speed. This is the sound speed that an isothermal cylinder with this spatial distribution of gas would have. This sound speed is then compared to the actual one in order to identify the isothermal segments. We designate as isothermal those segments with ratios within a factor of two of 1.0. As will be shown below, these segments arguably form a distinct population from the others. Out of a total of 618 candidates 87 are isothermal.

To make a more accurate assessment we eliminate overlaps. Overlapping can occur because a given gas particle can be part of a segment issuing from more than one galaxy. Because of possible misalignments with the radial directions from the centers of the galaxies in question, the quality of the fitting of a region may differ depending upon which galaxy it is considered to have emanated from. For each segment, then, we determine what fraction of the gas particles are not held in common with other segments with better fits. For this procedure, the measure of fit was taken as the absolute value of the deviation from one of the ratio of the square of the actual and effective sound speeds.

The segments, weighted by their non-overlapping fractions, are added together to form the histograms that follow and Table 1. In the scatter plots that follow, only segments whose non-overlapping fractions exceed one half are included.

For the isothermal-like segments a histogram of the square of ratio of the average actual sound speed to the effective one shows a peak at 1.0 (Figure 9, dotted, black line with filled circles).

After the elimination of overlaps, the 618 candidates are reduced to the equivalent of 540 non-overlapping segments, of which 117 are isothermal-like. Among the isothermal-like the equivalent of 71 are isothermal.

The total mass per unit length of an isothermal cylinder is

$$\frac{2c_s^2}{G} \quad (5)$$

where c_s is the sound speed and G is the gravitational constant. For a typical segment with a temperature of 1-2 times 10^4 K, this mass is about $4 \times 10^8 M_\odot$ of gas. Typically a large galaxy is surrounded by two to three filaments. The parent shell of a segment would then need a minimum of about $10^9 M_\odot$ of total gas to accommodate 2.5 isothermal cylinders. Not all of the parent shells even have this much gas.

The scatter plot in Figure 10 compares the sound speed ratio to the total cosmic overdensity of the parent shell. All of the points represent isothermal-like segments. Those that have gas fractions greater than one half are enclosed in green diamonds. As the shell overdensity falls below ten the sound speed ratio rises indicating that there is too little gas to balance the ambient temperature.

Figure 9 shows that this density effect accounts for most of the the failure of isothermal-like segments to be isothermal. The dashed, blue line with squares shows the

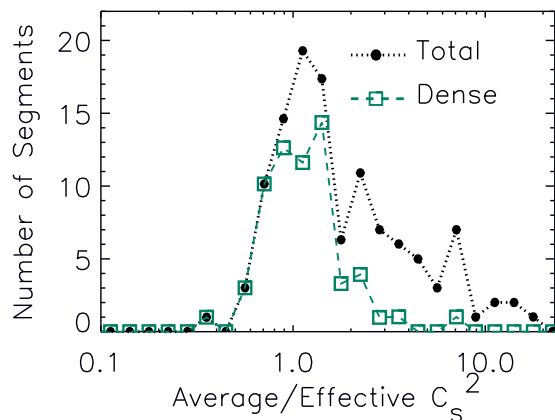


Figure 9. Comparison of the ratio of the squares of the actual and effective sound speeds for the isothermal-like segments (dotted, black line with filled circles) and for the subset from parent shells having a total overdensity greater than ten (dashed, blue line with squares). Overlaps have been eliminated for this figure.

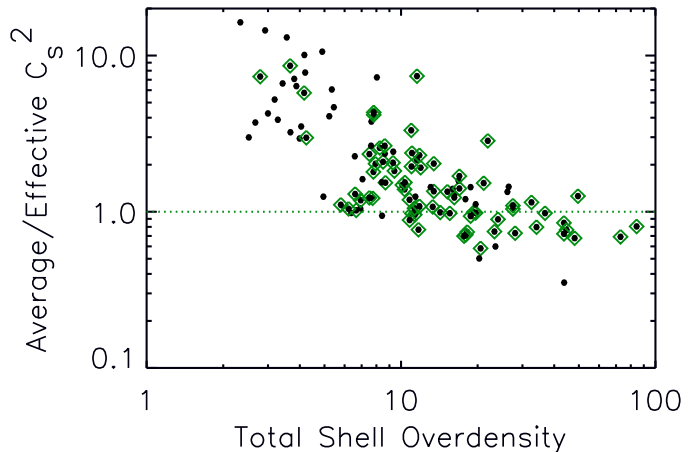


Figure 10. Ratio of the square of the average actual sound speed to the that of the effective one as a function of total overdensity of the parent shell. All of the points represent isothermal-like segments. Those that have gas fractions greater than one half are enclosed in green diamonds. Dotted green line marks a ratio of one.

sound speed ratio distribution for segments whose parent shells have a total cosmic overdensity of at least ten.

Another factor that might be important is the gas fraction of the segment. Dark matter might increase the gravitational field enough to accommodate a higher temperature, or it might disrupt the isothermal structure altogether. Figure 11 shows the ratio of the square of the sound speeds of the isothermal-like segments as a function of gas fraction. All of the points represent isothermal-like segments. Those that have parent shell overdensities greater than ten are enclosed

Table 1. Numbers of Segments. Fractions are by numbers of segments or by gas mass (in parentheses). Overlaps have been eliminated as described in section 4.6

Criterion	Total	Isothermal	Isothermal/Total
None	540	71	0.13 (0.30)
Density	135	55	0.41 (0.52)
Density and Gas Fraction	81	42	0.52 (0.64)

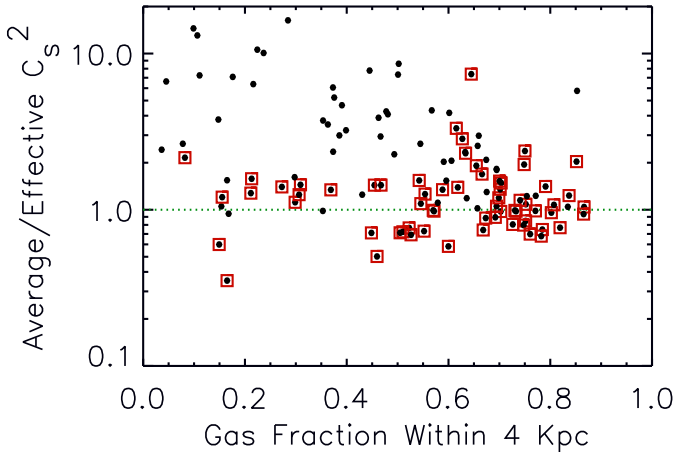


Figure 11. Ratio of the square of the average actual sound speed to the that of the effective one as a function of the gas fraction within four kpc. All of the points represent isothermal-like segments. Those that have parent shell overdensities greater than ten are enclosed in red boxes. Dotted, green line marks a ratio of one.

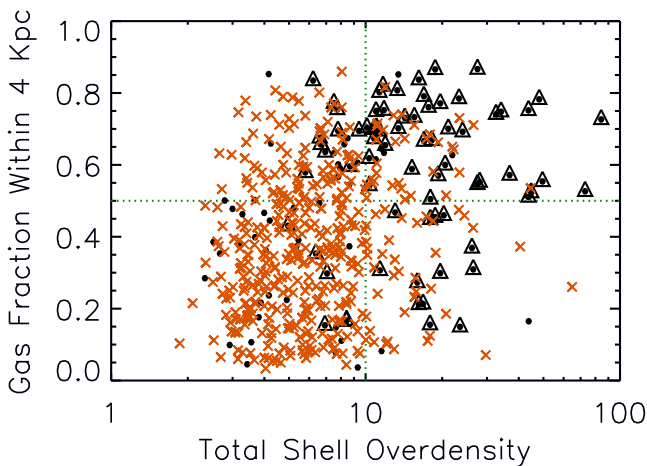


Figure 12. Gas fraction within 4 kpc versus total parent shell overdensity. Filled black circles are the isothermal-like segments. Those of the isothermal-like segments that are isothermal are enclosed in black triangles. Orange X's show candidate segments that are not isothermal-like. Dotted green line marks a ratio of one.

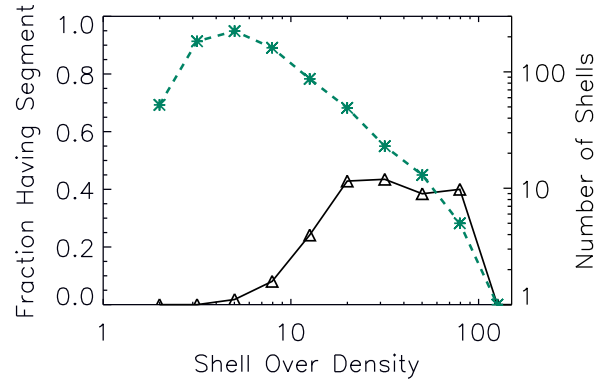


Figure 13. Occupation of shells by isothermal cylinders. The dashed, blue line with stars is a histogram of the overdensities of the shells in our study. The solid, black line with triangles shows the fraction of shells having at least one isothermal segment.

in red boxes. This figure shows that higher gas fractions are more conducive to isothermal cylinders.

Figure 12 combines the two criteria of overdensity and gas fraction. The upper right quadrant of the figure contains those segments that have both a parent shell of overdensity greater than ten and a gas fraction greater than one half. In this quadrant, 42 of the 81 candidates are isothermal segments, that is, those for which the potential profile matches that of an isothermal cylinder with an effective sound speed squared within a factor of two of the actual one. The statistics from this graph are summarized in Table 1.

Despite our efforts to qualify segments, isothermal cylinders might still fail to make the final cut for a variety of reasons. In addition to misalignment and extraneous structures nearby, some of the segments might have a scale radius too small or too large to be modeled in our study. With these considerations in mind, we conclude that isothermal cylinders are at least common among filament segments residing in regions conducive to the formation of these structures.

The isothermal segments are among the most massive filaments we have identified and thus would be expected to be avenues of transport for a disproportionately large fraction of the gas. With this in mind, Table 1 shows the fractions by gas mass in parentheses.

Figure 13 shows that among the densest shells, those with an overdensity greater than twenty, about 40% have at least one isothermal segment.

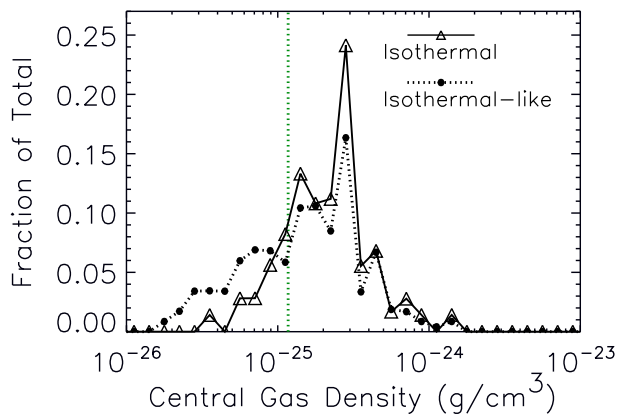


Figure 14. Computed central density of the isothermal and isothermal-like segments. The abscissa is the gas density in grams per cubic centimeter. The dotted, green line shows the gas density that would correspond, by itself without dark matter, to a cosmic overdensity of 200. Isothermal segments are indicated by the solid line with triangles. Isothermal-like segments by the dotted line with filled circles.

4.7 Central Density

The scale radius and the effective sound speed together determine the central density of an isothermal cylinder. Figure 14 shows that the central gas densities of the isothermal segments peak at about 500 times the overall cosmic density. The dotted, green line marks a density of 200 times. For comparison, the density at the radius of the inflection point of the isothermal potential profile is reduced from the central one by only a factor of four. These results argue that in most cases the gas alone provides enough gravitational field to keep the filament collapsed in an expanding cosmos. Many of the segments to the left of the green line are isothermal-like segments with too little gas to be isothermal.

5 CONCLUSIONS AND DISCUSSION

We conclude that a plausible model for intergalactic filaments at redshift 5 is an isothermal gas cylinder whose structure and stability are determined primarily by the gravitational and hydrodynamic properties of the gas. The cylinders have a central gas density of several hundred times the mean total cosmic density, with a peak at about 500. The average temperatures of the gas in the cylinders is 1-2 times 10^4 K.

Our findings fit well into the emerging picture of gas transport into galaxies. Except for galaxies larger than a few times $10^{11} M_{\odot}$ in mass at low redshifts, gas is believed to enter galaxies primarily through intergalactic filaments at temperatures well below the virial temperature of the galaxy and is never shock-heated (Birnboim & Dekel 2003; Katz et al. 2003; Kereš et al. 2005; Dekel & Birnboim 2006; Kawata & Rauch 2007; Ocvirk et al. 2008; Kereš et al. 2009; Dekel et al. 2009; Brooks et al. 2009). The temperatures of our filaments are below a few times 10^4 K, mostly

well below the estimated virial temperatures of the galaxies, which range from about 4×10^5 K down to about 3×10^4 K³.

Our findings for redshift 5 argue for a specific structure of the gas in filaments that is determined and stabilized primarily by the hydrodynamics of the gas. The proposed structure predicts, as a function of temperature, the maximum mass of gas that can be associated with a filament, a quantity that constrains the maximum star formation rate that may be achieved.

Many of the galaxies in the simulation, particularly small ones, do not have recognizable intergalactic filaments attached to them. For these galaxies the diffuse, hot, ionized gas around them may have few mechanisms to enter. Thus the presence or absence of filaments may effectively divide galaxies into two categories, those that can efficiently accrete gas and form stars and those that cannot. If the baryon-rich cores require a minimum amount of gas for the stability of an isothermal cylinder, it may be that the stellar content of a galaxy is a good indication for overall cosmic density. The importance of the gas environment for accretion has been emphasized by Kereš et al. (2005).

The dearth of satellite galaxies around the Milky Way is sometimes cited as a problem for the currently favored Λ CDM cosmology, which would predict many more satellite dark haloes. An absence of filaments at an earlier stage in cosmic history may have prevented these haloes from becoming luminous today. Whatever the explanation, it is worth noting that the simulation predicts a clear separation between gas and dark matter at the spatial dimensions of small galaxies. We would argue, then, that an assessment of the number of galaxies that form stars requires a simulation that at a minimum includes some gas hydrodynamics.

We invariably see our filaments embedded within thin sheets of gas. This observation suggests that the filaments might emerge from the sheets. Schmid-Burgk (1967) has shown that an infinite isothermal cylinder is but one extreme of a series of isothermally balanced structures that range from the infinite isothermal sheet, through intermediate structures containing regularly spaced, parallel, embedded filaments with elliptical cross-sections, to the other extreme of isolated cylinders.

A hydrodynamic origin of the filaments may help to explain a general difference between the collapse of dark matter and gas in our simulation. The dark matter can collapse only so far into filaments before fragmenting and collapsing further into spheroidal structures. The gas on the other hand can collapse into denser filaments which are stable to small perturbations.

ACKNOWLEDGMENTS

We are grateful to Nickolay Y. Gnedin for providing the output from the simulation, his visualization software IFRIT, and helpful comments on the final manuscript.

³ The virial temperatures were computed using a spherically symmetric mass profile within the virial radius of the galaxy.

REFERENCES

- Birnboim Y., Dekel A., 2003, MNRAS, 345, 349
- Brooks A. M., Governato F., Quinn T., Brook C. B., Wadsley J., 2009, ApJ, 694, 396
- Dekel A., Birnboim Y., 2006, MNRAS, 368, 2
- Dekel A., Birnboim Y., Engel G., Freundlich J., Goerdt T., Mumcuoglu M., Neistein E., Pichon C., Teyssier R., Zinger E., 2009, Nature, 457, 451
- Gnedin N. Y., 1995, ApJS, 97, 231
- Gnedin N. Y., Baker E. J., Bethell T. J., Drosback M. M., Harford A. G., Hicks A. K., Jensen A. G., Keeney B. A., Kelso C. M., Neyrinck M. C., Pollack S. E., van Vliet T. P., 2003, ApJ, 583, 525
- Gnedin N. Y., Bertschinger E., 1996, ApJ, 470, 115
- Gnedin N. Y., Fan X., 2006, ApJ, 648, 1
- Górski K. M., Hivon E., Banday A. J., Wandelt B. D., Hansen F. K., Reinecke M., Bartelmann M., 2005, ApJ, 622, 759
- Harford A. G., Gnedin N. Y., 2003, ApJ, 597, 74
- Harford A. G., Gnedin N. Y., 2007, ApJ, 664, 599
- Harford A. G., Hamilton A. J. S., Gnedin N. Y., 2008, MNRAS, 389, 880
- Katz N., Keres D., Dave R., Weinberg D. H., 2003, in J. L. Rosenberg & M. E. Putman ed., The IGM/Galaxy Connection. The Distribution of Baryons at $z=0$ Vol. 281 of Astrophysics and Space Science Library, How Do Galaxies Get Their Gas. pp 185–191
- Kawata D., Rauch M., 2007, ApJ, 663, 38
- Kereš D., Katz N., Fardal M., Davé R., Weinberg D. H., 2009, MNRAS, 395, 160
- Kereš D., Katz N., Weinberg D. H., Davé R., 2005, MNRAS, 363, 2
- Ocvirk P., Pichon C., Teyssier R., 2008, MNRAS, 390, 1326
- Ostriker J., 1964, ApJ, 140, 1056
- Schmid-Burgk J., 1967, ApJ, 149, 727
- Stodólkiewicz J. S., 1963, Acta Astronomica, 13, 30